Classical and quantum chaos of the wedge billiard. I. Classical mechanics

T. Szeredi and D. A. Goodings
Department of Physics and Astronomy, McMaster University, Hamilton, Ontario, Canada L8S 4M1
(Received 2 December 1992)

In this first of two papers on the classical-quantum correspondence of the wedge billiard, the classical mechanics for wedge angles giving hard chaos is described. Attention is focused on the periodic orbits of the system, all of which are known to be unstable. Each primitive periodic orbit has been found to correspond uniquely to a sequence of two symbols, except for certain orbits of the 60° wedge that go directly into the vertex. However, not every binary sequence has a corresponding periodic orbit. A total of 1048 primitive periodic orbits of the 49° wedge and 1920 primitive periodic orbits of the 60° wedge have been found and their actions, Maslov indices, and stability exponents determined. The primitive periodic orbits of word length n have been used to calculate the mean action $\bar{S}(n)$, the mean Maslov index $\bar{\nu}(n)$, and the mean stability exponent $\bar{u}(n)$. To a good approximation, each of these quantities increases linearly with n. It is also shown that there exist families consisting of many or possibly an infinite number of primitive periodic orbits with nearly the same action.

PACS number(s): 05.45.+b, 03.20.+i, 03.65.−w

I. INTRODUCTION

This is the first of two papers concerned with the classical and quantum behavior of a system which we call the "wedge billiard"—a particle in a wedge acted on by a constant force parallel to one side of the wedge. Of central interest is the correspondence between the trajectories of the classical particle and the energy eigenvalues and eigenfunctions of the analogous quantum system. Among the many questions that may be asked concerning this correspondence, two are of particular interest. First of all, is it possible to obtain a good approximation to the eigenvalues and eigenfunctions of the quantum system if one knows only the classical trajectories? Conversely, what can the energy eigenvalues and eigenfunctions tell one about the classical motion?

It will be shown in the following paper that for wedge angles such that the classical motion is strongly chaotic (in the sense that nearby trajectories diverge exponentially for almost all initial conditions), partial answers to both questions may be obtained using the well-known periodic orbit theory developed by Gutzwiller [1–5] and Balian and Bloch [6], including recent extensions involving dynamical ζ functions [7–15]. In particular, a good approximation to the energy eigenvalues of the quantum system can be obtained by recasting the Gutzwiller trace formula [4] as a ζ product and finding the zeros of the "functional determinant" [12–19], as will be described in detail in the second paper.

An essential ingredient for these studies is detailed knowledge of those special classical trajectories that close on themselves—the periodic orbits of the system. The present paper describes an extensive investigation of the periodic orbits of the wedge billiard. Although motivated by the classical-quantum correspondence and the Gutzwiller trace formula, we have found many properties of these orbits that are of interest in their own right. First, as described in Sec. III, each primitive periodic orbit is associated with a unique sequence of symbols (and their cyclic permutations), but not every sequence of symbols corresponds to a periodic orbit. This has important implications for the cycle expansions [10, 11] of the dynamical ζ function. We have also found that there are infinite families of primitive periodic orbits having very nearly the same action, as described in Sec. V. The existence of such families means that pseudo-orbit expansions of the dynamical ζ function [12, 16] cannot be implemented in a straightforward manner. Furthermore, since the accumulation point for each such family is not "isolated," it is questionable whether these families of orbits can be treated by the stationary-phase approximation which underlies the Gutzwiller trace formula. Finally, in Sec. VI we consider some scaling properties of the actions, Maslov indices, and stability exponents.

II. THE WEDGE BILLIARD

The wedge billiard consists of a particle confined to the region between the y axis and the line $y = x \cot \phi$ where ϕ is the wedge angle. The particle makes elastic collisions with the sides of the wedge and is acted upon by a constant force in the negative y direction. The Hamiltonian is

$$H = \frac{1}{2}(p_x^2 + p_y^2) + y, \qquad x > 0, \quad y > x \cot \phi. \tag{1}$$

The motion of a classical billiard in a symmetric wedge has been studied by Lehtihet and Miller [20] and by Richter, Scholz, and Wittek [21]. Furthermore, Wojtkowski [22] has shown that the desymmetrized wedge is related by a canonical transformation to the system consisting of two balls in one dimension with gravity studied by Whelan, Goodings, and Cannizzo [23].

One of the attractive features of the wedge billiard is that for different values of the wedge angle ϕ it shows different types of behavior. For $0° < \phi < 45°$ the sys-

tem exhibits Kolmogorov-Arnold-Moser (KAM) behavior, that is, surfaces of section show islands of stability (KAM tori) embedded in seas of chaos. For $\phi = 45°$ the system is classically integrable and the Schrödinger equation may be solved by separation of variables. For $45° < \phi < 90°$ the system has been proven to exhibit hard chaos, that is, there are no KAM tori in the phase space and all trajectories are unstable [22,24]. Thus, it is possible to study transitions between KAM behavior, integrable behavior, and hard chaos by varying the wedge angle.

Since the potential of the wedge billiard is homogeneous [meaning that $V(\lambda x, \lambda y) = \lambda V(x,y)$], it follows [25] that if one is given a trajectory at some energy E', one can find the trajectory at some other energy E by setting

$$x(t) = \left(\frac{E}{E'}\right) x'(t'), \quad p_x(t) = \left(\frac{E}{E'}\right)^{1/2} p'_x(t'), \tag{2}$$

$$y(t) = \left(\frac{E}{E'}\right) y'(t'), \quad p_y(t) = \left(\frac{E}{E'}\right)^{1/2} p'_y(t'), \tag{3}$$

$$t = \left(\frac{E}{E'}\right)^{1/2} t'. \tag{4}$$

We shall always work at $E' = 1$, knowing that the trajectories at any other energy can be obtained by scaling the coordinates, momenta, and time using these relations.

III. PERIODIC ORBITS

Nearly a century ago Poincaré [26] recognized the importance of the periodic orbits of a classical system in the context of chaotic motion. To find them in a systematic way, however, is not an easy task. One possible approach, described by Richter, Scholz, and Wittek [21], is to determine systematically the intersections of Birkhoff's symmetry lines in a suitably chosen Poincaré surface of section. However, this algorithm does not yield periodic orbits with "broken symmetries," which in the case of the wedge billiard are known to exist. (They correspond to periodic orbits which are not self-retracing.)

The approach we have used employs a symbolic description which provides a unique label for each periodic orbit. Each periodic orbit consists of n symbols taken from a two-letter *alphabet* [11] T and V, where n corresponds to the number of reflections of the billiard from the tilted wall of the wedge during one traversal of the orbit. If the billiard strikes the vertical boundary of the wedge between two successive reflections from the tilted wall, the bounce is labeled by V. If it does not hit the vertical wall between successive reflections from the tilted wall, it is labeled by T. The sequence of symbols describing a periodic orbit will be called a *word*, and the number of symbols in the sequence will be called the *word length*. Clearly, cyclic permutations of the letters in a word correspond to the same periodic orbit. Likewise, the reversed sequence of letters, corresponding to traversing the periodic orbit in the opposite direction, will be considered to belong to the same periodic orbit. Examples of periodic orbits of the wedge billiard are shown in Fig. 1.

Those words which do not consist of repetitions of shorter words correspond to *primitive periodic orbits*. The symbol γ will be used to label a primitive periodic orbit. Multiple traversals of a given primitive periodic orbit will be taken into account explicitly in the Gutzwiller trace formula and the dynamical ζ functions in the following paper.

We have found, as a result of thousands of calculations, that an arbitrary nonrepeating sequence of letters T and V (and their cyclic permutations) either yields a unique primitive periodic orbit or that no such orbit exists. In the latter case, the word is said to be *pruned* by the dynamics [11]. Our numerical method for finding the orbits is based on a two-dimensional Newton-Raphson iterative process, which is described in the Appendix. For the 60° wedge we have found all the primitive periodic orbits with word length ≤ 15, plus many others having longer word lengths. Similar calculations have also been carried out for wedge angles of 46°, 49°, and 55°. It turns out that the amount of pruning depends strongly on the wedge angle.

For each primitive periodic orbit γ one needs to know five properties: the action S_γ, the period T_γ, the stability exponent u_γ, the sign of the trace of the monodromy matrix σ_γ, and the Maslov index ν_γ. The action and period at energy E are given by

$$S_\gamma(E) = \oint \mathbf{p} \cdot d\mathbf{q}, \qquad T_\gamma(E) = \frac{\partial S_\gamma(E)}{\partial E}. \tag{5}$$

Then from the scaling relations of Eqs. (2)–(4) one finds

$$S_\gamma(E) = E^{3/2} S_\gamma(1), \tag{6}$$

$$T_\gamma(E) = (3/2) E^{1/2} S_\gamma(1) = E^{1/2} T_\gamma(1). \tag{7}$$

Thus, once a primitive periodic orbit has been deter-

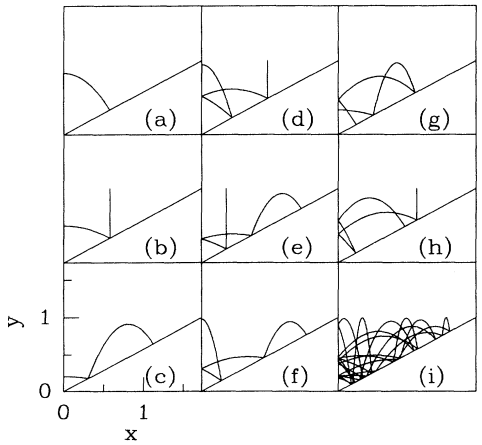

FIG. 1. Examples of primitive periodic orbits of the 60° wedge. (a) V; (b) TV; (c) TTV; (d) TVVV; (e) TTVTV; (f) TTVVV; (g) TVVTV; (h) TVVVV; (i) TTTVTVTVVTVTTVVV.

mined at unit energy, the action $S_\gamma(1)$ can be calculated by summing the contributions from all the parabolic arcs making up the orbit, and, from Eq. (7), the period at unit energy is given by $T_\gamma(1) = (3/2)S_\gamma(1)$.

The stability index u_γ of a primitive periodic orbit is calculated by a method similar to that described by Gutzwiller [4]. This involves calculating the monodromy matrix M_γ at some point on the primitive periodic orbit. Knowing the analytical form of the T and V mappings, we can calculate analytically the 3×3 monodromy matrices for single T and V bounces, which are just the Jacobean matrices of the mappings. Then, for a given primitive periodic orbit, the 3×3 monodromy matrix for one traversal of the orbit is obtained by multiplying the corresponding sequence of single-bounce matrices together. Since, when the wedge angle ϕ is greater than 45°, all periodic orbits are unstable [20,22–24], the eigenvalues of M_γ are always real and their product is equal to unity. One eigenvalue is always unity while the other two are reciprocally related. Then the stability exponent u_γ is defined to be the natural logarithm of the magnitude of the largest eigenvalue of M_γ. We have found this method of calculating u_γ to be more accurate numerically than the one described by Gutzwiller [4] involving a 2×2 monodromy matrix. It should be added that u_γ does not change under a rescaling of the energy, i.e., $u_\gamma(E) = u_\gamma(1)$.

In addition to u_γ, the Gutzwiller trace formula and its various reformulations require, in the case of hard chaos, the sign of the trace of the monodromy matrix, which is denoted by σ_γ. When $\sigma_\gamma = +1$, the mapping referred to above is hyperbolic, whereas $\sigma_\gamma = -1$ corresponds to a map that is hyperbolic with inversion.

In the case of a trajectory which goes precisely into the wedge vertex, without colliding with either wall, the calculation of u_γ is not straightforward. This is because an initially connected piece of phase space $(\delta q_2, \delta p_2)$ surrounding the trajectory as it enters the vertex becomes broken into two pieces which separate macroscopically after the collision with the vertex. Thus, the phase flow bifurcates as a result of the vertex collision. If such a trajectory were part of a primitive periodic orbit, the stability exponent u_γ would be effectively infinite. Such periodic orbits do not contribute to the Gutzwiller trace formula and, therefore, can be omitted from further consideration.

Although orbits that go directly into the wedge vertex usually do not contribute to the trace formula and its extensions, an exception occurs for the 60° wedge. It was pointed out by Smilansky [27] that in this special case, when the billiard goes into the wedge vertex at an angle of 60° to the horizontal, it emerges from the vertex at exactly the same angle, even when the billiard misses the vertex by a small amount and makes a collision with either the vertical (V) or the tilted (T) wall close to the vertex. This interesting special case is illustrated in Fig. 2, which shows the primitive periodic orbits TVV for the 59° wedge and TTTV for the 61° wedge. In the limit as $\phi \to 60°$ from either above or below, both primitive periodic orbits become the same, as shown in Fig. 2(c). Note, however, that u_γ approaches the value 2.06 for the TVV orbit as $\phi \to 60°$ from below, whereas it approaches the value 2.29 for the TTTV orbit as $\phi \to 60°$ from above.

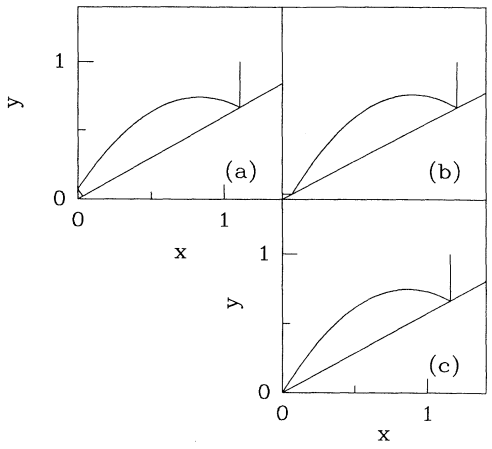

FIG. 2. (a) TVV for the 59° wedge; (b) TTTV for the 61° wedge; (c) the "vertex orbit" for the 60° wedge. This primitive periodic orbit is approached by the two preceding orbits when the wedge angle approaches 60°.

Other "vertex orbits" of the 60° wedge have been found for which the phase space surrounding the trajectory does not bifurcate following the collision with the vertex. Several of these are shown in Fig. 3. In each case the trajectories entering and leaving the vertex make equal angles with the wedge bisector, a property that is easy to prove analytically. Since each of the "vertex orbits" of the 60° wedge is a limiting case approached from above and below by primitive periodic orbits having different words, it is not possible to label each one by a unique sequence of T's and V's. This unusual situation means that cycle expansions and pseudo-orbit expansions (to be described in the following paper) cannot be carried out in a straightforward manner.

Finally, an important feature of a primitive periodic or-

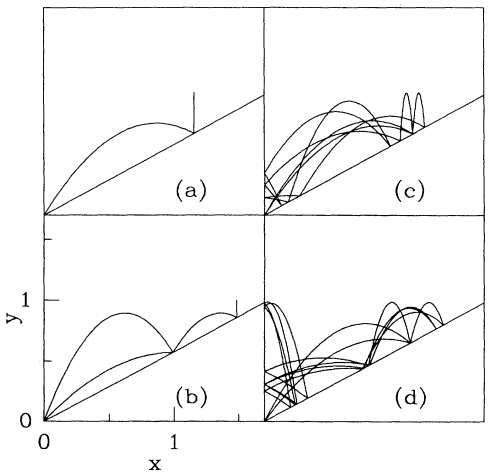

FIG. 3. Four different "vertex orbits" of the 60° wedge. Each is a limiting case corresponding to $\phi \to 60°$ from above and below.

TABLE I. The primitive periodic orbits of the 60° wedge having word length less than 8.

Word	S_γ	u_γ	ν_γ	σ_γ
V	1.33333	0.69315	5	-1
TV	2.30940	1.31696	8	-1
TTV	2.91043	1.84725	11	-1
TVV	3.26592	2.06344	13	1
TTTV	3.26605	2.29243	14	-1
TVVV	4.81335	2.70228	18	-1
TTVTV	5.11682	3.17631	19	1
TTVVV	5.17881	3.23281	21	-1
TVTVV	5.72342	3.33168	21	-1
TVVVV	6.04658	3.42841	23	1
TTTVTV	5.33333	3.63689	22	1
TTTVVV	5.35747	3.67832	23	-1
TTVTVV	6.12133	3.86858	24	-1
TTVVVV	6.30282	3.99942	26	1
TVTVVV	7.15829	4.01700	26	1
TVVVVV	7.43158	4.09913	28	-1
TTTTVTV	5.44331	4.02503	25	1
TTTTVVV	5.45431	4.05543	26	-1
TTTVTTV	6.14577	4.14288	25	1
TTTVTVV	6.31210	4.31946	27	-1
TTVTVTV	7.45669	4.48526	27	-1
TTVTVVV	7.60035	4.55449	29	1
TTVVVVV	7.74065	4.64527	31	-1
TVTVTVV	7.99802	4.66284	29	1
TVTVVVV	8.43790	4.72135	31	-1
TVVTVVV	8.12000	4.74020	31	-1

TABLE II. The primitive periodic orbits of the 49° wedge having word length less than 9.

Word	S_γ	u_γ	ν_γ	σ_γ
V	1.04323	0.48474	5	-1
TV	1.92931	0.94360	8	-1
TVV	2.59555	1.48123	13	1
TTVV	2.73807	1.96982	16	1
TVVV	3.91283	1.90729	18	-1
TTTVV	2.79379	2.39554	19	1
TVVVV	4.80835	2.42951	23	1
TTTTVV	2.82076	2.76202	22	1
TTVVVV	5.06856	2.89745	26	1
TVTVVV	5.86979	2.85203	26	1
TVVVVV	5.94909	2.88177	28	-1
TTTTTVV	2.83574	3.07970	25	1
TTTVVVV	5.19034	3.31098	29	1
TTVVTVV	5.35298	3.44742	29	1
TTVVVVV	6.33795	3.30081	31	-1
TVTVTVV	6.60327	3.33199	29	1
TVVTVVV	6.60732	3.34294	30	-1
TVVVVVV	6.93500	3.38853	33	1
TTTTTTVV	2.84489	3.35826	28	1
TTTTVVVV	5.25490	3.67028	32	1
TTTVVTVV	5.43049	3.86883	32	1
TTVVVVVV	7.24360	3.84261	36	1
TVTVTVVV	7.78708	3.79668	34	-1
TVVTVVVV	7.42104	3.90429	36	1
TVVVVVVV	8.01449	3.85663	38	-1

bit is its Maslov index [5], denoted by ν_γ. In the next section we describe how this was determined by the method recently proposed by Creagh, Robbins, and Littlejohn [28]. For future reference, Tables I and II give the calculated values of $S_\gamma(1)$, u_γ, ν_γ, and σ_γ for all the primitive periodic orbits up to word length 6 for the 49° wedge and the 60° wedge. [Recall from Eq. (7) that the period is given by $T_\gamma(1) = (3/2)S_\gamma(1)$.]

IV. CALCULATION OF THE MASLOV INDICES

In the Gutzwiller trace formula and the dynamical ζ functions, the contribution from each primitive periodic orbit γ involves the phase factor $\exp(-i\nu_\gamma\pi/2)$, where ν_γ is the Maslov index. In the original derivation of the trace formula, Gutzwiller [4] introduced a coordinate system in which q_1 is directed along the orbit and q_2 is perpendicular to it at each point. (We shall specialize to a system with two degrees of freedom.) Let us denote an initial point on a primitive periodic orbit by (q_1', p_1'), with $q_2' = p_2' = 0$ by definition. Now suppose that a pencil of trajectories, having a range of momentum components p_2' spread about $p_2' = 0$, starts out from this point at $t = 0$. At a later time t the set of trajectories will have, in general, a range of position coordinates q_2. A *conjugate point* is defined to occur whenever it happens that, at some instant of time, $\partial q_2/\partial p_2' = 0$. Each time such a point is encountered in traversing a periodic orbit, the Maslov index is increased by unity. In addition, the Maslov index has a contribution determined by the sign of

$$\Xi = \frac{1}{2}\left(\frac{\partial^2 S}{\partial q_2' \partial q_2'} + 2\frac{\partial^2 S}{\partial q_2' \partial q_2''} + \frac{\partial^2 S}{\partial q_2'' \partial q_2''}\right), \tag{8}$$

which enters the second variation of $S(q', q'', E)$ away from the periodic orbit. Here q_2'' is the q_2 coordinate after one traversal of the orbit. Depending on whether Ξ is positive or negative one adds 0 or 1 to ν_γ.

Figure 4 suggests a method of determining ν_γ for a given primitive periodic orbit that is in the spirit of Gutzwiller's original paper. In a manner similar to an illustration given by Creagh, Robbins, and Littlejohn [28] for a primitive periodic orbit of the stadium billiard, we show in Fig. 4(a) and Fig. 4(b) that the number of conjugate points may be different for different starting points on the orbit. Nevertheless, because the expression in (8) has opposite signs at these two different starting points, the final result for ν_γ is the same.

Recently Creagh *et al.* proposed a different method for calculating the Maslov index of a primitive periodic orbit. Starting from an arbitrary point on the orbit, one follows the direction of the unstable manifold in the (q_2, p_2) plane as it winds around the orbit during a single traversal. (The direction of the unstable manifold at a given time t may be found by calculating the eigenvalues and eigenvectors of the 2×2 monodromy matrix at time t.) If θ is the angle between one direction of the unstable manifold and the q_2 axis, then as the orbit is traversed it steadily decreases, corresponding to a clockwise rotation of the unstable manifold in the (q_2, p_2) plane. In addition there occur discontinuous changes in θ each time

there is a collision with the boundary. (The jump in θ is exactly $\pm 180°$ if the collision is at right angles to the boundary.) For a system that does not have collisions with hard boundaries (represented by an infinite potential jump), the method proposed by Creagh *et al.* is to set ν_γ equal to the number of times the chosen direction of the unstable manifold crosses the p_2 axis in the (q_2, p_2) plane, either at $\theta = 90°$ or at $\theta = -90°$. In addition, ν_γ is to be incremented by unity each time the particle velocity is zero. When there are hard-wall collisions, as in billiard problems, ν_γ must be further incremented by 2 for each collision. In all the calculations reported in this and the following paper, the Maslov indices were calculated according to this prescription.

To illustrate the method, results of calculations of θ as a function of t for the primitive periodic orbit TTV of the 60° wedge are shown in Fig. 5. Figures 5(a) and 5(b) correspond to the two starting points of Figs. 4(a) and 4(b). In both plots of θ against t there occur four discontinuous jumps, corresponding to collisions with the wedge boundary, and three "slow" crossings of θ with the dashed lines at 90° and −90°, leading to the value $\nu_\gamma = 11$. This result is, of course, in agreement with the method based on counting the number of conjugate points and the sign of Ξ, provided ν_γ is likewise incremented by 2 for each collision with the boundary.

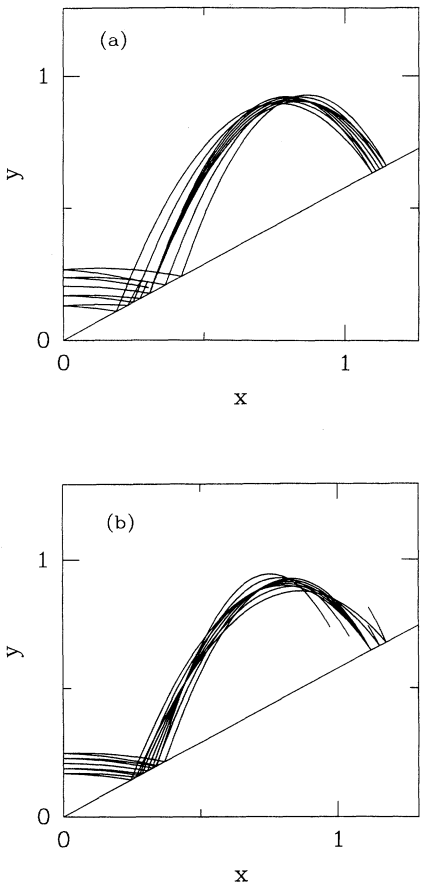

FIG. 4. Pencils of trajectories starting out from different points on the primitive periodic orbit TTV of the 60° wedge and followed through one traversal of the orbit. (a) The starting point is low on the tilted wall. On the upward trajectory, a focal point occurs just to the right of the maximum. After being reflected from the tilted wall, a caustic occurs near the maximum on the way back. For this starting point, $\Xi = -4.3$. (b) The starting point is high on the tilted wall. Now there are two focal points and one caustic. The first focal point occurs just to the left of the first maximum, the second well to the left of the maximum near the end of the orbit. The caustic occurs close to the maximum near the end of the orbit. In this case $\Xi = 3.9$. Note that all the trajectories in (a) and (b) have been computed for the same length of time.

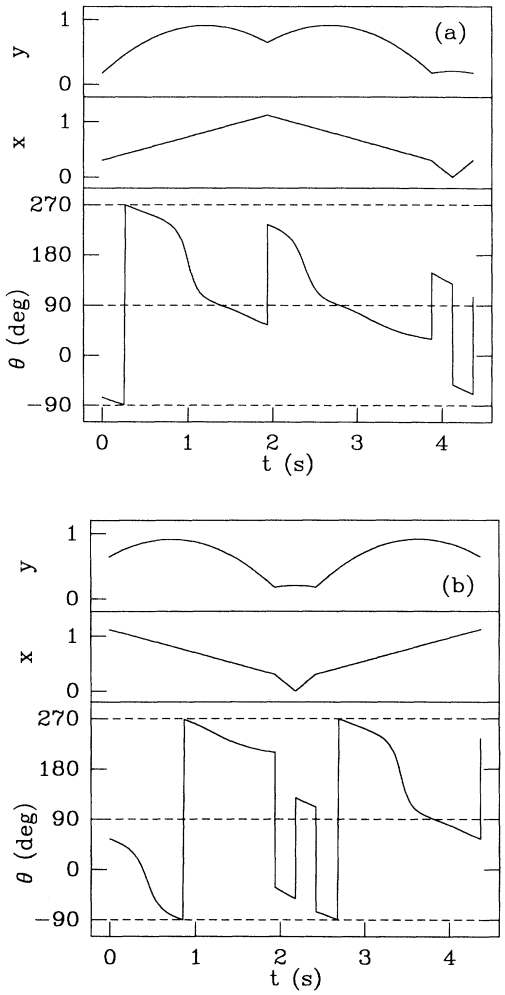

FIG. 5. The angle θ that the unstable manifold makes with the p_2 axis as a function of the time t, followed through one period of the primitive periodic orbit TTV of the 60° wedge. Above the θ plot, the x and y coordinates of the trajectory are plotted as a function of t. (a) and (b) correspond to the two different starting points in the preceding figure. Note that each of the four collisions with the walls produces a discontinuous jump in θ. Note also that after the final collision with the tilted wall, θ differs by 180° from its initial value, indicating that the primitive periodic orbit TTV is hyperbolic with reflection.

V. FAMILIES OF PRIMITIVE PERIODIC ORBITS

An interesting feature of the classical motion of the wedge billiard is that there occur families containing many or possibly an infinite number of primitive periodic orbits having nearly the same action. The existence of these families is evident from Fig. 6, which shows the stability exponent u_γ plotted against the corresponding action S_γ for many primitive periodic orbits of the 49° wedge and the 60° wedge. Each vertical spike on these plots corresponds to a family of primitive periodic orbits. For each family the least upper bound of the actions is called an *accumulation point*, which will be denoted by S_∞. Similar bounded families of primitive periodic orbits have been found to occur in the anisotropic Kepler problem [18, 19] and also as the "whispering gallery modes" of the stadium billiard [29].

Typical families of primitive periodic orbits of the 49° and 60° wedges are listed in Tables III–VI. For each family, the words, actions, stability exponents, and Maslov indices of several primitive periodic orbits are given. For certain families, including the $T^mVVTTVV$ family of the 49° wedge and the T^mVVV family of the 60° wedge, the limiting value of the stability exponent has been found to be infinite, as Tanner and Wintgen [18] found in the case of one such family in the anisotropic Kepler problem.

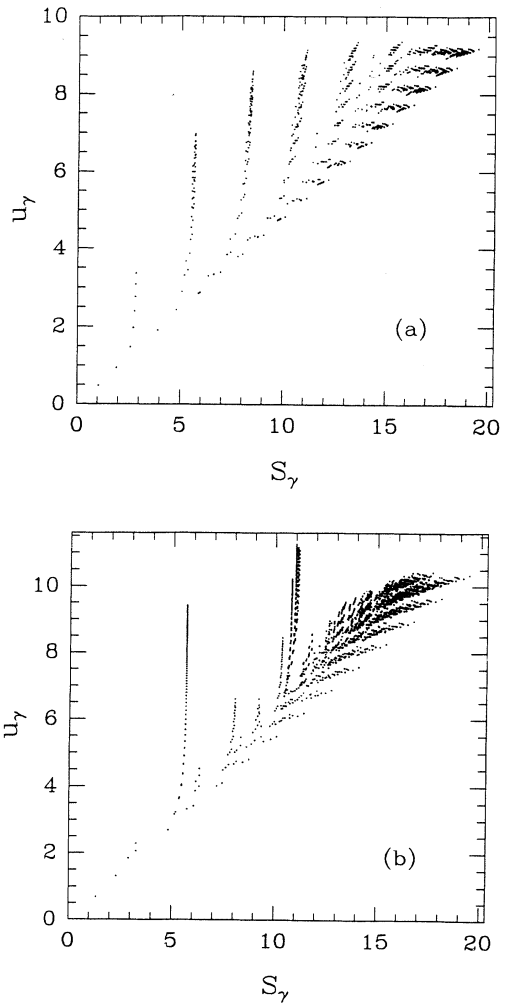

FIG. 6. The stability exponents u_γ plotted against the corresponding actions S_γ: (a) for 1048 primitive periodic orbits of the 49° wedge; (b) for 1920 primitive periodic orbits of the 60° wedge. (Forward and backward directions count as one orbit.)

TABLE III. The family of primitive periodic orbits $T^mVVTTVV$ of the 49° wedge.

m	S_γ	u_γ	ν_γ	σ_γ
3	5.53595	4.36452	35	1
4	5.56836	4.72983	38	1
5	5.58756	5.04659	41	1
6	5.59976	5.32448	44	1
7	5.60795	5.57112	47	1
8	5.61370	5.79235	50	1
9	5.61787	5.99265	53	1
10	5.62100	6.17546	56	1
11	5.62340	6.34349	59	1
12	5.62529	6.49887	62	1
13	5.62679	6.64334	65	1
14	5.62800	6.77829	68	1
15	5.62900	6.90487	71	1
16	5.62983	7.02404	74	1
17	5.63053	7.13661	77	1
18	5.63112	7.24327	80	1
19	5.63163	7.34459	83	1
20	5.63207	7.44108	86	1
21	5.63245	7.53317	89	1
22	5.63278	7.62125	92	1
23	5.63307	7.70564	95	1
24	5.63332	7.78664	98	1
25	5.63355	7.86452	101	1
26	5.63375	7.93949	104	1
27	5.63394	8.01177	107	1
28	5.63410	8.08154	110	1
29	5.63425	8.14898	113	1

One family of the 60° wedge consists of primitive periodic orbits of the form $TTT\cdots TVVV$. Four members of this family, which we shall denote as T^mVVV, are

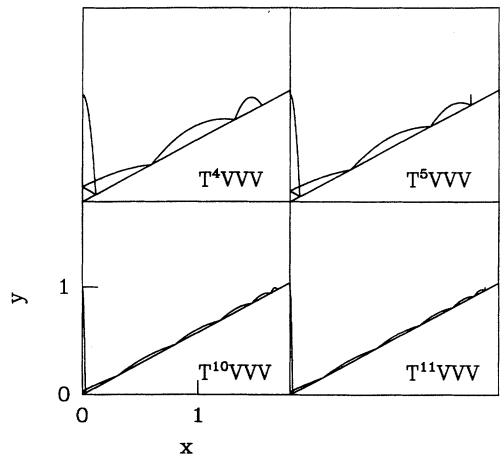

FIG. 7. Four members of the family T^mVVV for the 60° wedge.

shown in Fig. 7. A typical primitive periodic orbit moves down the tilted wall making several T bounces, enters the velocity-reversing sequence VVV near the wedge vertex, and then retraces its path of T bounces up the tilted wall.

TABLE IV. The family of primitive periodic orbits T^mVVV of the 60° wedge.

m	S_γ	u_γ	ν_γ	σ_γ
1	4.81335	2.70228	18	-1
2	5.17881	3.23281	21	-1
3	5.35747	3.67832	23	-1
4	5.45431	4.05543	26	-1
5	5.51162	4.37939	29	-1
6	5.54799	4.66194	32	-1
7	5.57239	4.91174	35	-1
8	5.58949	5.13521	38	-1
9	5.60192	5.33715	41	-1
10	5.61123	5.52119	44	-1
11	5.61837	5.69017	47	-1
12	5.62396	5.84630	50	-1
13	5.62843	5.99136	53	-1
14	5.63204	6.12679	57	-1
15	5.63501	6.25377	59	-1
16	5.63748	6.37327	62	-1
17	5.63955	6.48612	65	-1
18	5.64131	6.59301	69	-1
19	5.64282	6.69454	72	-1
20	5.64411	6.79120	74	-1
21	5.64524	6.88344	77	-1
22	5.64622	6.97165	80	-1
23	5.64708	7.05616	83	-1
24	5.64785	7.13727	86	-1
25	5.64852	7.21523	89	-1
26	5.64913	7.29028	92	-1
27	5.64967	7.36264	95	-1
28	5.65015	7.43248	98	-1
29	5.65059	7.49997	101	-1
30	5.65099	7.56527	104	-1
31	5.65135	7.62851	107	-1
32	5.65167	7.68983	110	-1
33	5.65197	7.74932	113	-1
34	5.65225	7.80710	116	-1
35	5.65250	7.86326	119	-1
36	5.65273	7.91790	122	-1
37	5.65294	7.97108	124	-1
38	5.65314	8.02290	128	-1
39	5.65333	8.07340	130	-1
40	5.65350	8.12267	134	-1
41	5.65365	8.17075	136	-1
42	5.65380	8.21771	140	-1
43	5.65394	8.26359	143	-1
44	5.65406	8.30844	146	-1
45	5.65418	8.35232	149	-1
46	5.65430	8.39525	152	-1
47	5.65440	8.43728	155	-1
48	5.65450	8.47845	158	-1
49	5.65459	8.51879	161	-1
50	5.65468	8.55833	164	-1
55	5.65505	8.74512	179	-1
60	5.65534	8.91597	194	-1
65	5.65556	9.07337	209	-1
∞	5.65685	∞	∞	-1

TABLE V. The family of primitive periodic orbits $T^mVVVTTTTVVV$ of the 60° wedge.

m	S_γ	u_γ	ν_γ	σ_γ
6	11.00116	8.71800	60	1
7	11.02489	8.96820	63	1
8	11.04143	9.19200	66	1
9	11.05341	9.39421	69	1
10	11.06234	9.57847	72	1
11	11.06918	9.74763	75	1
12	11.07453	9.90390	78	1
13	11.07880	10.04909	81	1
14	11.08225	10.18462	84	1
15	11.08508	10.31168	87	1
16	11.08743	10.43126	90	1
17	11.08940	10.54417	93	1
18	11.09107	10.65111	96	1
19	11.09250	10.75268	99	1
20	11.09373	10.84938	102	1
21	11.09480	10.94166	105	1
22	11.09574	11.02990	108	1
23	11.09656	11.11444	111	1

As the number of T bounces tends to infinity, the action approaches that of a path which starts at $x = \tan\phi$, $y = 1$, moves along the tilted wall to the vertex, rises along the vertical wall to $y = 1$, and then retraces its motion back to the starting point. For this limiting case, the action is found to be $2^{5/2} = 5.65685$. This "limiting orbit" is *nonisolated* in the following sense: given an arbitrary point on the orbit, any neighborhood of this point in phase space will contain points belonging to other primitive periodic orbits having nearly the same action. This has important consequences for the Gutzwiller trace formula which will be explored in the following paper.

It should be noted that families of primitive periodic

TABLE VI. The family of primitive periodic orbits $T^mVTVTTTTVTV$ of the 60° wedge.

m	S_γ	u_γ	ν_γ	σ_γ
6	10.98939	8.66910	56	1
7	11.01578	8.92246	59	1
8	11.03418	9.14849	62	1
9	11.04751	9.35233	65	1
10	11.05746	9.53782	68	1
11	11.06507	9.70792	71	1
12	11.07103	9.86493	74	1
13	11.07578	10.01071	77	1
14	11.07962	10.14672	80	1
15	11.08277	10.27418	83	1
16	11.08539	10.39408	86	1
17	11.08759	10.50727	89	1
18	11.08946	10.61445	92	1
19	11.09105	10.71622	95	1
20	11.09242	10.81309	98	1
21	11.09361	10.90552	101	1
22	11.09465	10.99389	104	1
23	11.09556	11.07854	107	1
24	11.09637	11.15977	110	1

orbits, in which the actions approach a limiting value as n increases, occur for all wedge angles. As another illustration we show in Fig. 8 four primitive periodic orbits of the family T^mVVTTVV of the 49° wedge.

It is natural to ask whether there is an infinite number of such infinite families at every wedge angle. Since we do not know of a systematic way of generating such families (for example, by adding T^m to a given word), we are unable to answer this question.

The existence of infinite families of primitive periodic orbits of the type we have been considering implies that one cannot define a "topological entropy" for the wedge billiard. In other systems that exhibit hard chaos the number of primitive periodic orbits is known to grow exponentially with the length of the orbit or its action. Numerical studies of the Hadamard-Gutzwiller model of a particle moving freely on a surface of constant negative curvature [30] and of the hyperbola billiard [31] have found excellent agreement with the asymptotic form,

$$N(l) \underset{l\to\infty}{\sim} \frac{\exp(\tau l)}{\tau l}, \tag{9}$$

where $N(l)$ is the number of primitive periodic orbits γ having length $l_\gamma \leq l$, and τ is called the *topological entropy*. Since for these billiard systems, at constant energy, the action of a primitive periodic orbit is just $S_\gamma = pl_\gamma$, where p is the constant magnitude of the momentum, a relationship similar to that above can be written for $N(S)$, the number of primitive periodic orbits with actions $S_\gamma \leq S$. It is natural to ask whether such a relation holds for the wedge billiard. The answer, however, is clearly no because of the infinite families of orbits described in this section. For the same reason, a relationship of the form of Eq. (9) does not exist for the anisotropic Kepler problem, as has been noted by Gutzwiller [5].

Although the topological entropy does not exist for the wedge billiard, it is possible to define, by analogy, a *word length entropy* τ_w. Let $N(n)$ denote the number of primitive periodic orbits having word length n. Then τ_w is defined by

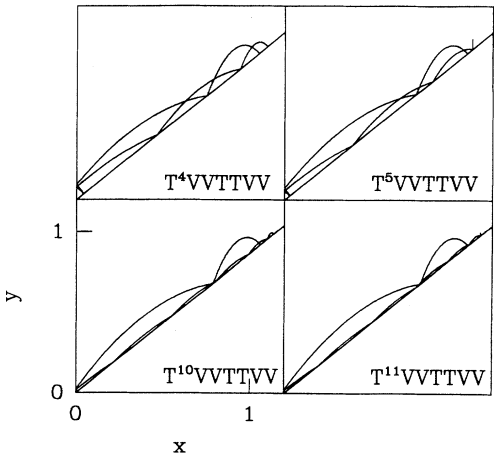

FIG. 8. Four members of the family T^mVVTTVV for the 49° wedge.

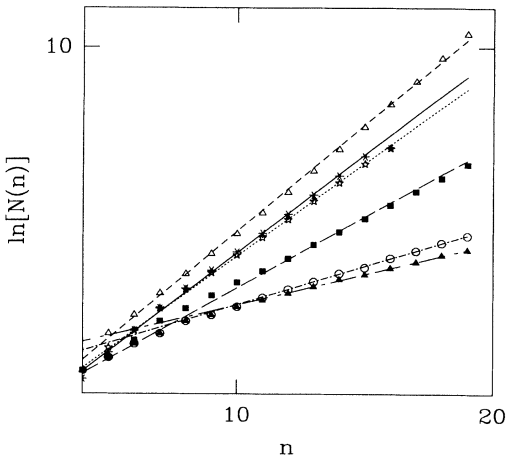

FIG. 9. The natural logarithm of the number of primitive periodic orbits of word length n plotted against n for different wedge angles. Medium-dashed line: unpruned dynamics, $\tau_w = 0.554$; solid line: 60° wedge, $\tau_w = 0.510$; dotted line: 55° wedge, $\tau_w = 0.482$; long-dashed line: 49° wedge, $\tau_w = 0.368$; medium dashed-dot line: 46° wedge, $\tau_w = 0.199$; long dashed-dot line: 45.5° wedge, $\tau_w = 0.159$.

$$N(n) \underset{n\to\infty}{\sim} \exp(\tau_w n). \tag{10}$$

The number of physically existing primitive periodic orbits of word length n has been determined using the method described in the Appendix as far as $n = 15$ or higher, for each of the wedge angles 60°, 55°, 49°, 46°, and 45.5°. The results are given in Fig. 9, which shows that there is an approximate straight-line relationship at each wedge angle, confirming the form of Eq. (10). The straight line with the largest slope in Fig. 9 corresponds to a nonexistent wedge such that every unique sequence of T's and V's (after removing cyclic permutations, time-reversed sequences, and repeated cycles) corresponds to a primitive periodic orbit—in other words, there is no pruning. By comparison, one sees that there is a significant amount of pruning even for the 60° wedge, and the amount of pruning increases rapidly as ϕ approaches 45°.

VI. SCALING PROPERTIES

With the pseudo-orbit expansions and the cycle expansions of the dynamical ζ function very much in mind (see the following paper), we examine in this section how various properties of the primitive periodic orbits scale with the word length n. In Fig. 10 the mean value of the actions for primitive periodic orbits having word length n, denoted $\bar{S}(n)$, is plotted against n. Plots are shown for four different wedge angles. In each case $\bar{S}(n)$ increases approximately linearly with n. It is also interesting to study how the actions at a fixed value of n are distributed about $\bar{S}(n)$. A histogram of the actions S_γ for all the primitive periodic orbits of word length 15 for the 60° wedge is shown in Fig. 11. The distribution is approximately Gaussian. Similar distributions have been

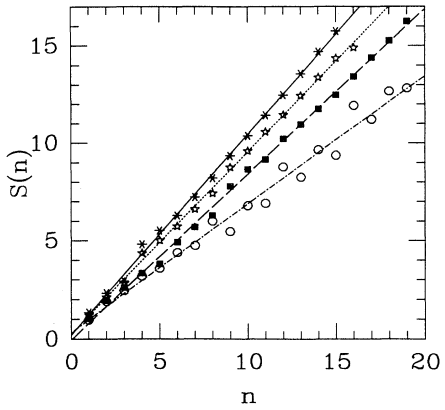

FIG. 10. The mean action $\bar{S}(n)$ of primitive periodic orbits of word length n plotted against n for different wedge angles. Solid curve: 60° wedge; dotted curve: 55° wedge; dashed curve: 49° wedge; dot-dashed curve: 46° wedge.

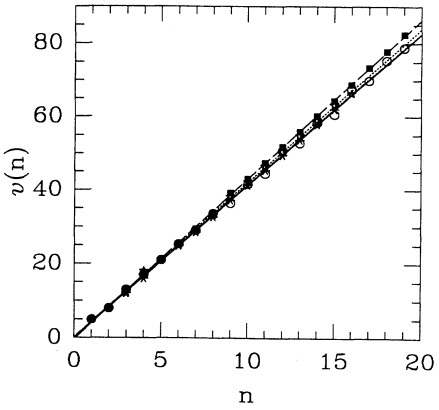

FIG. 12. The mean Maslov index $\bar{\nu}(n)$ of primitive periodic orbits of word length n plotted against n for different wedge angles. The curves are identified as in Fig. 10.

found at other values of n for both the 49° wedge and the 60° wedge [32]. Szeredi has also shown that, for a given wedge angle, the normalized distributions are almost identical when plotted, for each n, in terms of the dimensionless variable $S_\gamma(n)/\bar{S}(n)$.

Figure 12 shows the average Maslov index for the primitive periodic orbits of word length n, denoted $\bar{\nu}(n)$, plotted against n. Plots for different wedge angles are almost indistinguishable on this plot. Here too one finds a linear relation to a good approximation.

In Fig. 13 we show a plot of the mean stability exponent, $\bar{u}(n)$, against n for four different wedge angles. Again there is a remarkably good linear relation.

Closely related to the mean stability exponent is the mean Lyapunov exponent $\bar{\lambda}(1)$, for energy $E = 1$, defined by

$$\bar{\lambda}(1) = \frac{1}{N}\sum_{\gamma=1}^{N}\frac{u_\gamma}{T_\gamma(1)}, \tag{11}$$

where $T_\gamma(1)$ is the period of the primitive periodic orbit γ, as in Eq. (7), and N is the number of primitive periodic orbits in the sum over γ. Using 1819 primitive periodic orbits of the 60° wedge (forward and backward directions count as one orbit), we found $\bar{\lambda}(1) = 0.417$. This is to be compared with the value $\bar{\lambda}(1) = 0.425$ determined for a very long chaotic trajectory of the 60° wedge calculated from an arbitrary initial point of the $E = 1$ phase space. [The calculation was performed by following the trajectory through many T and V mappings until the largest eigenvalue of the 3×3 monodromy matrix had grown larger than 10^{14}. $\bar{\lambda}(1)$ was then found by averaging over the values obtained from many such segments.] It is satisfying that the two values of $\bar{\lambda}(1)$ are in close agreement.

VII. DISCUSSION AND CONCLUSIONS

In this paper we have focused our attention on the primitive periodic orbits of the wedge billiard. It is often stated that the primitive periodic orbits provide a framework for the complete dynamics of a conservative dynam-

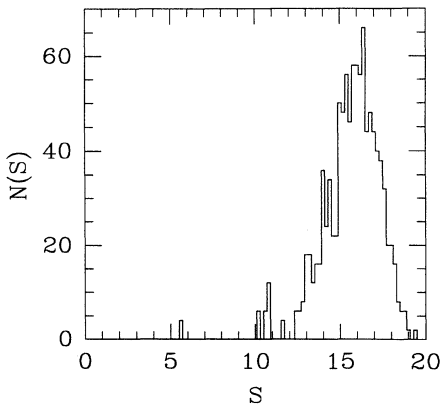

FIG. 11. Histogram of the actions of the primitive periodic orbits with $n = 15$ for the 60° wedge.

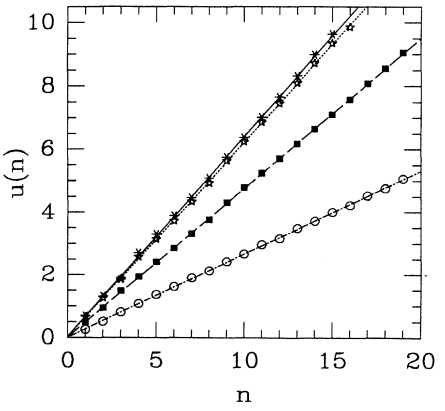

FIG. 13. The mean stability exponent $\bar{u}(n)$ of primitive periodic orbits of word length n plotted against n for different wedge angles. The curves are identified as in Fig. 10.

ical system. Figures 14 and 15 lend additional support to this claim. Figure 14 shows the Poincaré surface of section corresponding to the y and p_y components of the particle (with $p_x > 0$) at the instant just after a collision with the tilted wall. The 37 903 points in the figure were calculated from a single trajectory. The boundary enclosing the points was determined by conservation of energy. Figure 15 shows a similar plot containing the same number of points, but in this case the points were generated by 1819 primitive periodic orbits of the 60° wedge. Some of the pronounced lines and curves in this plot can be interpreted as mappings of the symmetry lines described by Richter, Scholz, and Wittek [21]. The streaks in the lower part of the plot arise from some of the infinite families described in Sec. V. It is clear that the primitive periodic orbits are distributed almost everywhere in the allowed region. It is also noticeable that there are some empty regions. However, these must eventually be filled in by points from primitive periodic orbits of longer word length, since the periodic orbits are densely distributed among all possible trajectories in the phase space. The ribbon devoid of points running beside the lower boundary corresponds to orbits with many T bounces, but other pointless regions are not so easy to interpret. Despite these empty regions, it is fair to say that the motion of the particle in the constant energy phase space is well characterized by the primitive periodic orbits.

Our main findings may be briefly summarized. There exists a symbolic dynamics, consisting of two symbols, which uniquely describes each primitive periodic orbit (except for the "vertex orbits" of the 60° wedge). The search routine for primitive periodic orbits is firmly based on knowing the sequence of T's and V's for a given orbit. We have found that many possible words do not correspond to physical primitive periodic orbits, and the amount of pruning increases as the wedge angle approaches 45°. An important feature of the wedge billiard is the existence of families of primitive periodic orbits having very nearly the same action, probably containing an infinite number of members. Finally, we have found that the mean values of the action, the Maslov index,

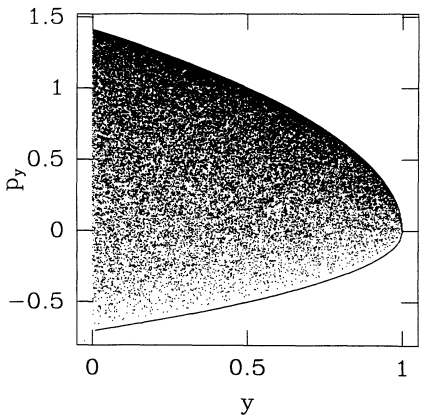

FIG. 14. Poincaré surface of section corresponding to the y and p_y components of the particle just after a collision with the tilted wall. The 37 903 points were generated by a single trajectory of the 60° wedge.

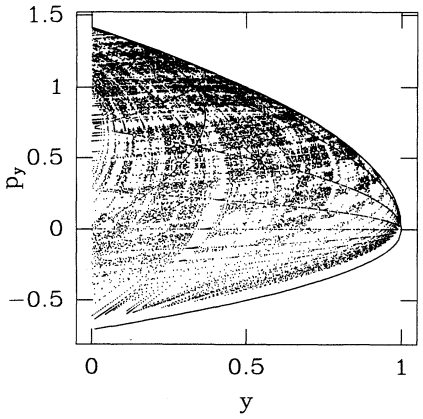

FIG. 15. Poincaré surface of section similar to that in Fig. 14 with 37 903 points generated by 1819 primitive periodic orbits of the 60° wedge.

and the stability exponent increase approximately linearly with the word length n. These results are important for the study of the classical-quantum correspondence described in the following paper.

ACKNOWLEDGMENTS

We are very grateful to U. Smilansky for pointing out the existence of the special "vertex orbit" of the 60° wedge. We would also like to thank R.G. Littlejohn for helpful correspondence regarding the calculation of the Maslov indices. This research was supported by the Natural Sciences and Engineering Research Council of Canada.

APPENDIX

In this appendix the method used to find the primitive periodic orbit corresponding to a specified sequence of T's and V's is outlined.

First, the individual T and V maps must be specified. Following Lehtihet and Miller [20], we define the variables,

$$X = (\tan\phi)p_x + p_y, \tag{A1}$$

$$Y = (\cot\phi)p_x - p_y, \tag{A2}$$

where p_x and p_y are the components of the momentum of the particle just after a collision with the tilted wall. Conservation of energy for $E = 1$ leads to the requirement that

$$\frac{1}{2}[\cos^2(\phi)X^2 + \sin^2(\phi)Y^2] + r\cos\phi = 1, \tag{A3}$$

where we have put $y = r\cos\phi$. If X and Y are known, this relation can be used to find r, which locates the position of the collision with the tilted wall. From the equations of motion of the particle it is a straightforward matter to derive the T and V maps from an initial X_i,

Y_i to a final X_f, Y_f. The map for the T bounce is

$$X_f = X_i + 2Y_i, \qquad Y_f = Y_i, \tag{A4}$$

while the V bounce is given by

$$X_f = -X_i - Y_i + Y_f, \tag{A5}$$

$$Y_f = -[4 + 2\xi(X_i + Y_i)^2 - Y_i^2]^{1/2}, \tag{A6}$$

where $\xi = \cos(2\phi)\cos^2\phi$.

To find the initial conditions for a primitive periodic orbit corresponding to a specified sequence of T's and V's, the appropriate maps are carried out going from initial values X_i, Y_i to final values X_f, Y_f. The condition for a periodic orbit is that

$$X_f(X_i, Y_i) - X_i = 0, \quad Y_f(X_i, Y_i) - Y_i = 0. \tag{A7}$$

Finding the zeros of the functions on the left side of these equations was accomplished numerically using a two-dimensional Newton-Raphson method [33]. The search routine employed a 100×100 grid of starting values for X_i and Y_i. While many starting values do not lead to a solution, it was found that those that did always converged to the same result. However, since it was possible for one of the prescribed maps to carry the particle outside the wedge while still yielding a solution to Eq. (A7), it was important to check the solution X_i, Y_i to see if it gave a physical primitive periodic orbit. The final outcome of the search procedure is that a given sequence of T's and V's always led either to a unique primitive periodic orbit or to none at all.

[1] M.C. Gutzwiller, J. Math. Phys. **8**, 1979 (1967).
[2] M.C. Gutzwiller, J. Math. Phys. **10**, 1004 (1969).
[3] M.C. Gutzwiller, J. Math. Phys. **11**, 1791 (1970).
[4] M.C. Gutzwiller, J. Math. Phys. **12**, 343 (1971).
[5] M.C. Gutzwiller, *Chaos in Classical and Quantum Mechanics* (Springer-Verlag, New York, 1990).
[6] R. Balian and C. Bloch, Ann. Phys. (N.Y.) **69**, 76 (1972).
[7] M.C. Gutzwiller, J. Phys. Chem. **92**, 3154 (1988).
[8] M.V. Berry, in *Quantum Chaos and Statistical Nuclear Physics*, edited by T.H. Seligman and H. Nishioka, Lecture Notes in Physics Vol. 263 (Springer, Berlin, 1986), p. 1.
[9] A. Voros, J. Phys. A **21**, 685 (1988).
[10] P. Cvitanović and B. Eckhardt, Phys. Rev. Lett. **63**, 823 (1989).
[11] R. Artuso, E. Aurell, and P. Cvitanović, Nonlinearity **3**, 325 (1990).
[12] M.V. Berry and J.P. Keating J. Phys. A **23**, 4839 (1990).
[13] J.P. Keating, Proc. R. Soc. London Ser. A **436**, 99 (1992).
[14] E. Bogomolny, CHAOS **2**, 5 (1992).
[15] E. Bogomolny, Nonlinearity **5**, 805 (1992).
[16] M. Sieber and F. Steiner, Phys. Rev. Lett. **67**, 1941 (1991).
[17] G. Tanner, P. Scherer, E.B. Bogomolny, B. Eckhardt, and D. Wintgen, Phys. Rev. Lett. **67**, 2410 (1991).
[18] G. Tanner and D. Wintgen, CHAOS **2**, 53 (1992).
[19] F. Christiansen and P. Cvitanović, CHAOS **2**, 61 (1992).
[20] H.E. Lehtihet and B.N. Miller, Physica D **21**, 93 (1986).
[21] P.H. Richter, H.-J. Scholz, and A. Wittek, Nonlinearity **3**, 45 (1990).
[22] M.P. Wojtkowski, Commun. Math. Phys. **126**, 507 (1990).
[23] N.D. Whelan, D.A. Goodings, and J.K. Cannizzo, Phys. Rev. A **42**, 742 (1990).
[24] N.I. Chernov, Physica D **53**, 233 (1991).
[25] B. Eckhardt and E. Aurell, Europhys. Lett. **9**, 509 (1989).
[26] H. Poincaré, *Les Méthodes Nouvelles de la Mécanique Céleste* (Gauthier-Villars, Paris, 1892–1899).
[27] U. Smilansky (private communication). We are grateful to Professor Smilansky for drawing our attention to this special primitive periodic orbit and its finite stability exponent.
[28] S.C. Creagh, J.M. Robbins, and R.G. Littlejohn, Phys. Rev. A **42**, 1907 (1990).
[29] R.G. Littlejohn (private communication).
[30] R. Aurich and F. Steiner, Physica D **32**, 451 (1988).
[31] M. Sieber and F. Steiner, Physica D **44**, 248 (1990).
[32] T. Szeredi, Ph.D. thesis, McMaster University (1992) (unpublished).
[33] W.H. Press, B.P. Flannery, S.A. Teukolsky, and W.T. Vetterling, *Numerical Recipes* (Cambridge University Press, Cambridge, 1986), p. 269.